

# Single Qubit Bootstrapping and Gate Calibration

Julian Kelly

May 27, 2010

# Contents

<b>1</b>	<b>Introduction and Motivation</b>	<b>3</b>
<b>2</b>	<b>Qubit Frequency and First Order Tune-Up</b>	<b>3</b>
2.1	Frequency Mapping . . . . .	3
2.2	First Order $\pi$ -Pulse . . . . .	4
2.3	Ramsey Fringe . . . . .	5
2.4	Tracking the Qubit Frequency Precisely . . . . .	6
<b>3</b>	<b>Microwave Calibration: X &amp; Y Quadrature</b>	<b>8</b>
3.1	Phase Errors . . . . .	8
3.2	Amplified Phase Errors (APE) . . . . .	9
3.2.1	Phase Error Analysis . . . . .	9
3.2.2	Experimental Implementation . . . . .	12
3.3	Phase Error Correction . . . . .	13
3.3.1	Derivative Removal by Adiabatic Gate (DRAG) . . . . .	13
3.3.2	Half Derivative (HD) Method . . . . .	15
3.3.3	Caveats and Tunability . . . . .	16
<b>4</b>	<b>Quantum Process Tomography</b>	<b>17</b>
4.1	Formalism . . . . .	17
4.2	Experimentally Constructing $\chi$ . . . . .	18
<b>5</b>	<b>Flux Bias Calibration: Z control</b>	<b>19</b>
<b>6</b>	<b>Randomized Benchmarking</b>	<b>21</b>
6.1	Pulse Sequence . . . . .	21
6.2	Experimental Implementation & Analysis . . . . .	22
<b>7</b>	<b>Gate Timing</b>	<b>24</b>
<b>8</b>	<b>Conclusions &amp; Moving Forward</b>	<b>25</b>

# 1 Introduction and Motivation

High fidelity single qubit gates are integral to the operation of a quantum computer. Although decoherence may be the single greatest challenge in building such a computer, long coherence times are meaningless without a high degree of single qubit control. Before any computation or experiment can begin, it is critical to tune up individual qubits to find parameters such as frequency and nonlinearity, and to calibrate high fidelity gate operations.

The purpose of this thesis is to provide a user's manual on how to tune up a single Josephson phase qubit by fine tuning all relevant parameters and optimizing gate control. Here, I will outline a series of simple experiments that help to calibrate and check each qubit parameter, and conclude with a practical and scalable way of benchmarking single qubit operations. The good news is that all of these techniques should be 'for free', in the sense that they are all just software calibrations that do not require any new hardware or fabrication methods. Even better, many of these calibration experiments can be automated for speed and ease of use. As we start out knowing very little about the qubit, bootstrapping is an essential tool that puts a strict order to the experiments that we perform.

In order to make sure that we have high fidelity operations, we design metrological experiments that are sensitive to certain types of errors. We then use these experiments to measure and understand the errors while setting a benchmark for their correction.

This thesis also builds on current work in the field by extensively analyzing phase errors from qubit gates. The Amplified Phase Error (APE) sequence is developed and implemented in order to amplify and measure phase errors. In addition, the control theory Derivative Removal by Adiabatic Gate (DRAG) is modified for experiment as a tool for correcting phase errors and improving gate fidelity.

## 2 Qubit Frequency and First Order Tune-Up

### 2.1 Frequency Mapping

One thing that this thesis will not cover in depth is measurement techniques. For a phase qubit this involves SQUID calibration, readout and measurement pulses. For bringing up and calibrating these procedures, see the Ph.D thesis

of M. Ansmann *Benchmarking the Superconducting Josephson Phase Qubit - The Violation of Bell's Inequality*.<sup>1</sup>

The first and likely most important parameter sought after is the qubit frequency. Before any fine tuning is done, it is important to perform a 2-D spectroscopy to map out qubit frequency as a function of flux bias. This is done in order to avoid any stray two level systems (TLS). A  $T_1$  spectroscopy may also be performed to avoid any poor operating regions. Once an operating region has been pinned down, a 1-D spectroscopy can be done to find the qubit frequency to within a few MHz.

A high power 1-D spectroscopy can be done in order to excite the 2-photon  $|0\rangle - |2\rangle$  transition. This is related to  $f_{01}$ ,  $f_{12}$  and the nonlinearity  $\Delta$  in a simple way. The nonlinearity is defined as  $\Delta = 2\pi(f_{12} - f_{01})$ . Therefore, this 2-photon  $|0\rangle - |2\rangle$  transition is located exactly halfway between the frequencies  $f_{01}$  and  $f_{12}$ , as the total energy for this transition is  $hf_{02} = h(f_{01} + f_{12})$  and is split among two photons. This gives us a first measure of the nonlinearity.

## 2.2 First Order $\pi$ -Pulse

Now that we have some idea of the qubit frequency, we can tune up a simple  $\pi$ -pulse to use in an experiment that will measure the qubit frequency to high precision. Note that this  $\pi$ -pulse will have some substantial amplitude and phase errors, as it is just a first estimation. However, this can still be very useful for metrology as the experiment that we will use it in is insensitive to these kinds of errors.

This approximation to a  $\pi$ -pulse consists of a Gaussian envelope on the X-quadrature in the qubit frame, with time integrated area of  $\pi$  radians. A Gaussian is used as it minimizes the time it is active in the time domain, while also minimizing the non-essential frequencies that it excites in the frequency domain.

The amplitude can be tuned up by just sweeping the Gaussian amplitude from zero for a fixed length in time as shown in figure 1, until a maximum in the probability of the  $|1\rangle$  state is achieved. This will serve our purposes for now, as we just need large, but not necessarily perfect excitation of the qubit.

---

<sup>1</sup><http://www.physics.ucsb.edu/~martinisgroup/theses/Ansmann2009.pdf>

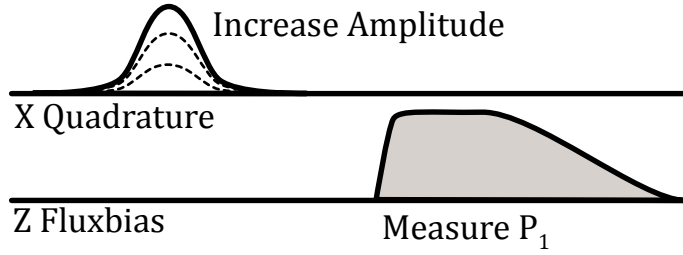


Figure 1: First Order  $\pi$ -Pulse tune up sequence.

### 2.3 Ramsey Fringe

The Ramsey fringe experiment is a very sensitive way of checking how well the qubit frequency is being tracked. The sequence, as shown in figure 2, is an  $X_{\pi/2}$ -pulse followed by some delay and ending with a second  $\frac{\pi}{2}$ -pulse with the microwave phase  $\theta$  swept from  $0 - 2\pi$ . Since we do not have finely tuned  $\frac{\pi}{2}$ -pulses yet, we may just use our first order  $\pi$ -pulse with the amplitude halved.

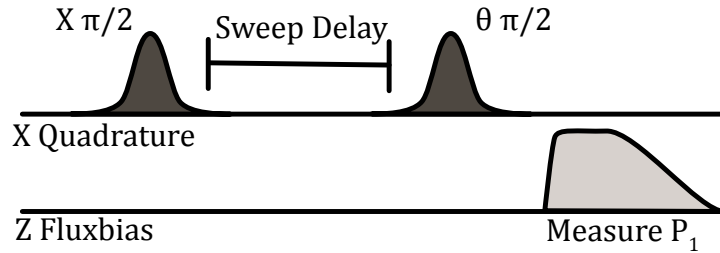


Figure 2: Ramsey fringe pulse sequence

As a baseline, we set the delay such that the pulses are well separated, and then sweep the phase of the second pulse to get a curve that should resemble  $P_1 = \cos \theta$ . Note that there are some phase errors in our  $\frac{\pi}{2}$ -pulse, as the  $|1\rangle$  state probability  $P_1$  is not always maximum at  $\theta = 0$  and minimum at  $\theta = \pi$ . However, we are not interested in these types of errors for this experiment. We will correct them later, as described in section 3.3.2 on page 15.

We are most interested in observing how these maxima and minima (or "fringes") change with delay between pulses. If we are exactly on resonance with the qubit frequency, these should be completely insensitive to the delay.

However, in reality we set our microwave signal to track the qubit frequency to ensure the correct phase on applied microwaves. If there is some error in frequency, we will see it manifest as the values of  $\theta$  for the maxima and minima in  $P_1$  change as a function of delay.<sup>2</sup> So, by sweeping the delay and  $\theta$  we can map out just how accurately we are tracking the qubit frequency.

At this point it is likely that we see some drift in the maxima and minima of  $P_1$ , as shown in figure 3. Using this experiment, it is easy to observe even a few MHz frequency error, for even an error of this size will be substantial when accrued through a typical qubit lifetime of  $T_1 = 500$  ns. An error of a mere 5 MHz can give a  $90^\circ$  phase error in just 100 ns, turning an X-pulse into a Y-pulse.

## 2.4 Tracking the Qubit Frequency Precisely

Now that we have a method for measuring small frequency errors, we must correct them. Although we could use the Ramsey fringe as outlined in the previous section as a way of correcting for these errors, there is a simple and easily scriptable solution that does not require a 2-D sweep. Using the following technique will allow us to lower frequency tracking errors to the  $10^{-5}$  range.

The frequency calibration experiment is a slightly modified Ramsey fringe. However, it is only a 1-D sweep so the calibration time is much faster. The pulse sequence is a X  $\frac{\pi}{2}$ -pulse followed by a second X  $\frac{\pi}{2}$ -pulse with the delay between them swept. However, the second pulse is tracking a frame processing at a slightly different frequency than the qubit.<sup>3</sup> This is equivalent to the axis of rotation for the second pulse to be rotating at a speed of the detuning with respect to the actual qubit frame. We choose 50 MHz as it provides well enough separated oscillations that allow us to determine the correction needed but is fast enough to avoid large decoherence errors.

When we measure  $P_1$ , we find that it oscillates at a frequency of around 50 MHz. Any deviation from the 50 MHz tells us exactly how far we are from the qubit frequency. We then adjust the microwave drive frequency until we

---

<sup>2</sup>Note how the phase errors mentioned previously are unimportant because we are only interested in the relative change in  $\theta$  as a function of delay, not the absolute values of  $\theta$  for the maxima and minima.

<sup>3</sup>It is important to note that the second pulse is on resonance with the qubit; only the frame tracking that affects the phase of the pulse is detuned.

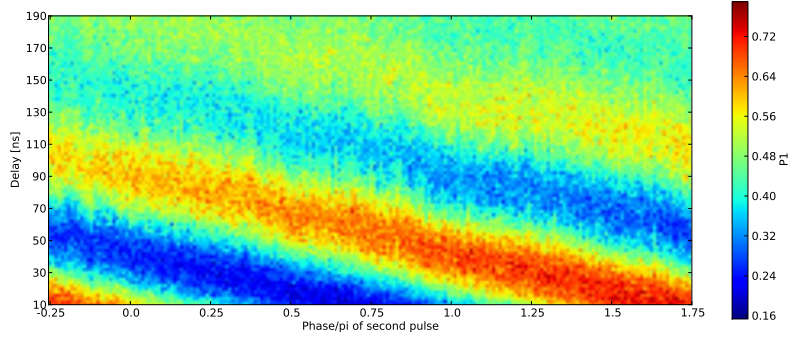


Figure 3: Ramsey Fringe - 10 MHz detuned. Note that the fringes are not constant in the vertical (delay) axis. This tells us that the fringes are not insensitive to delay, implying the microwave drive is not on resonance with the qubit frequency.

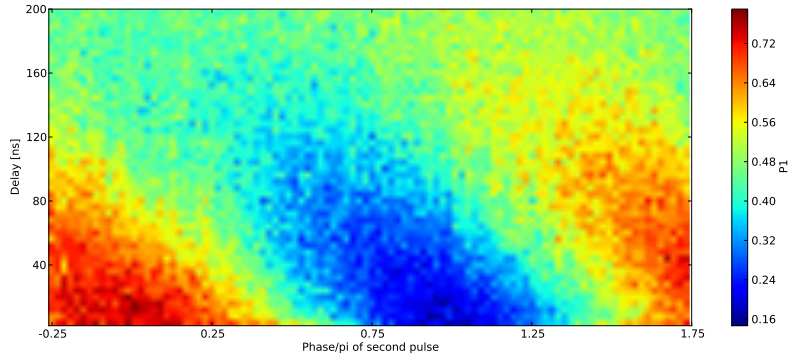


Figure 4: Ramsey Fringe - 2 MHz detuned. Again, we notice the fringes shifting with delay. Notice how sensitive this experiment is for even a 2 MHz detuning.

measure 50MHz oscillations as precisely as we can measure it.<sup>4</sup>

As a final check, shown in figure 6, we may perform a 2-D Ramsey fringe to confirm that we are sufficiently on resonance. Once we are confident in our measurement of  $f_{01}$ , we can use a similar technique to calibrate  $f_{12}$  by adding in a  $\pi$ -pulse to go from the  $|0\rangle$  to the  $|1\rangle$  state, and then perform the

<sup>4</sup>Note that this process is easily scriptable.

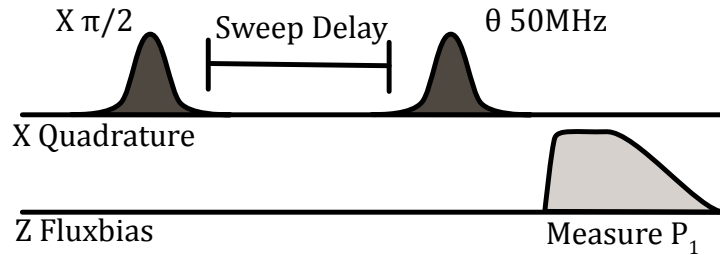


Figure 5: Frequency tuner pulse sequence

tune up procedure for the  $|1\rangle - |2\rangle$  transition as described previously. With both  $f_{01}$  and  $f_{12}$  we can easily calculate the nonlinearity  $\Delta$ .

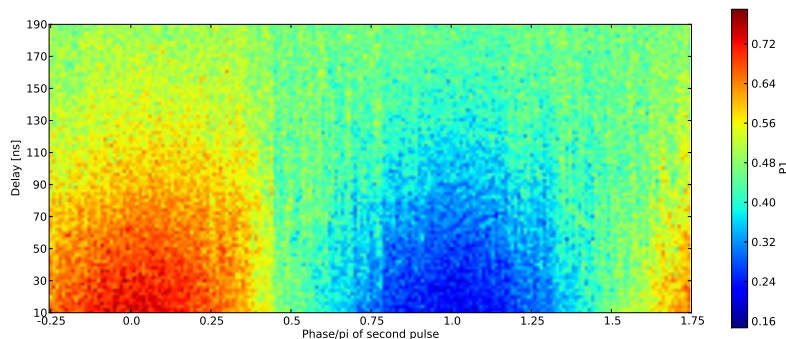


Figure 6: Ramsey Fringe - On Resonance. We see that the fringes locations are insensitive to the delay, showing us that we are on resonance.

### 3 Microwave Calibration: X & Y Quadrature

#### 3.1 Phase Errors

As we can see from figure 7, we notice that our initial calibration does not give a  $P_1$  with a maximum at  $\theta = 0$  and minimum at  $\theta = \pi$ . This is due to some phase error from our  $\frac{\pi}{2}$ -pulses. Due to the nature of our design, the qubit is not a perfectly ideal two level system. The presence of the  $|2\rangle$  state enables unwanted virtual transitions during qubit gates which results in a phase error.

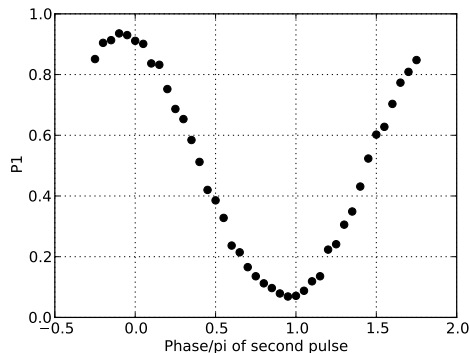


Figure 7: Ramsey Fringe - Phase Error

Given parameters for a fast gate, we find these phase errors to be around  $5^\circ - 10^\circ$ . This is a significant error, but also problematic because it is just large enough to cause substantial problems in long sequences, but small enough that it can be difficult to measure directly.

## 3.2 Amplified Phase Errors (APE)

We seek some method that will amplify this error in such a way that we can better measure it. In order to do this, we must investigate the nature of these errors and how they affect the gates.

### 3.2.1 Phase Error Analysis

We may model these errors in a simple way. Consider an ideal  $X_{\pi/2}$ -pulse given by the transformation

$$X_{\text{ideal}} = \frac{1}{\sqrt{2}} \begin{pmatrix} 1 & -i \\ -i & 1 \end{pmatrix} = e^{-i\sigma_x\pi/4}. \quad (1)$$

However, we find from experiment and simulations that a physical gate is modified in the following way:

$$X_{\text{physical}} = \frac{e^{-i\epsilon'}}{\sqrt{2}} \begin{pmatrix} 1 & -ie^{-i\epsilon} \\ -ie^{-i\epsilon} & e^{-2i\epsilon} \end{pmatrix}. \quad (2)$$

$$X_{\text{physical}} = e^{-i\epsilon'} Z_\epsilon X_{\text{ideal}} Z_\epsilon, \quad Z_\epsilon = \begin{pmatrix} 1 & 0 \\ 0 & e^{-i\epsilon} \end{pmatrix}, \quad (0 < \epsilon \ll 1), \quad (3)$$

where  $Z_\epsilon$  is the phase error generated from virtual transitions to the  $|2\rangle$  state. For the time being, we will ignore the global phase error  $\epsilon'$  as we are only concerned with single qubit gates.<sup>5</sup>

In the spirit of metrology, we look to construct a type of operation that will amplify and measure this  $\epsilon$  phase error without otherwise changing the state of the qubit. Consider two types of simple gate identities, one which consists of a net  $2\pi$  rotation by stringing together 4  $\frac{\pi}{2}$ -pulses, and one which is a positive, then negative  $\theta$  rotation. As is calculable from the error model in equation 3,  $X_{\text{physical}}^4 = -e^{-4i\epsilon} I$ ; the 4  $\frac{\pi}{2}$  pulses end up canceling out the  $\epsilon$  phase error that we are interested in. For this reason, we will explore the general  $\theta$  rotation identity more explicitly. Consider a general  $\theta$  rotation

$$X_\theta = \begin{pmatrix} \cos \frac{\theta}{2} & -i \sin \frac{\theta}{2} \\ -i \sin \frac{\theta}{2} & \cos \frac{\theta}{2} \end{pmatrix}. \quad (4)$$

Now, consider an identity using this transformation by concatenating a positive then negative<sup>6</sup>  $\theta$  rotation. For a first order expansion with  $\epsilon \ll 1$  we find

$$I_\theta = Z_\epsilon X_\theta^\dagger Z_\epsilon^2 X_\theta Z_\epsilon \approx I + \begin{pmatrix} i(\cos \theta - 1) & \sin \theta \\ -\sin \theta & -i(\cos \theta + 3) \end{pmatrix} \epsilon(\theta) + \mathcal{O}(\epsilon^2). \quad (5)$$

This result is complex, as  $\epsilon$  is a function of  $\theta$ . From simulation, we calculate  $\epsilon(\theta)$ , shown in figure 8. We notice that  $\epsilon$  increases monotonically up to  $\theta = \pi$ . However, given the form of  $I_\theta$ , we find that  $I_\pi = e^{-2i\epsilon} I$ ; the relative  $\epsilon$  error that we are interested in cancels out no matter the value of  $\epsilon$  as noted above. We accumulate a global phase error, but we are not interested in this at this time.

---

<sup>5</sup>It is important to note that global phase errors will become very important for multiple qubit experiments, however we seek a method of calibrating out these kinds of errors with only a single qubit. Fortunately, the method we develop seems to correct for global phase errors as well.

<sup>6</sup>Theoretically it is perfectly equivalent to do a negative, then positive  $\theta$  rotation. However, as described in section 3.2.2 it is experimentally desirable to do the opposite.

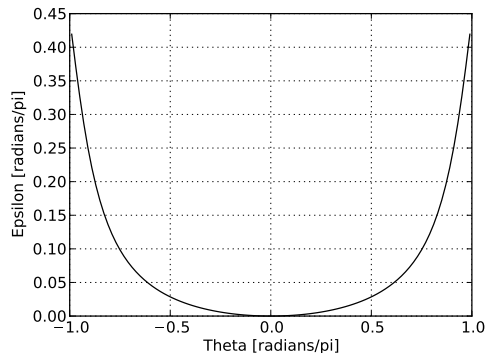


Figure 8:  $\epsilon$  Phase Error

To investigate the ideal value of  $\theta$ , consider a state that is sensitive to phase. We investigate  $I_\theta$  acting on that state and consider only the relative phase error  $\Delta\phi$ , defined by

$$|\psi\rangle = \frac{1}{\sqrt{2}} \begin{pmatrix} 1 \\ -i \end{pmatrix},^7 \quad I_\theta|\psi\rangle \approx \frac{1}{\sqrt{2}} \begin{pmatrix} 1 \\ -ie^{-i\Delta\phi} \end{pmatrix}.^8 \quad (6)$$

$\Delta\phi$  is an experimentally significant value, as it is generated from  $\epsilon$  and is physically present in the qubit state. We can plot the relative phase error  $\Delta\phi(\theta)$  from simulation which combines  $\epsilon(\theta)$  from figure 8 and  $I_\theta$  from equation 5, shown in figure 9.

Although the maximum is at  $\theta \approx 0.65$ , for experimental convenience we restrict ourselves to a  $\frac{\pi}{2}$ -pulse. We sacrifice roughly 20% of phase error generation, but ensure that we are using well defined and calibrated pulses. For  $\theta = \frac{\pi}{2}$ , we find

$$I_{\pi/2} = I + \begin{pmatrix} -i\epsilon & \epsilon \\ -\epsilon & -3i\epsilon \end{pmatrix} + \mathcal{O}(\epsilon^2). \quad (7)$$

Using the  $I_{\pi/2}$  operation we can generate  $\Delta\phi = 2\epsilon$  phase error. We must now develop an experiment that allows us to use this operation to generate a phase error that we can measure.

<sup>7</sup>It is important to note that  $|\psi\rangle$  must be located on the Y or -Y axis, as  $I_\theta$  rotates about the X axis.

<sup>8</sup>Again, we neglect global phase.

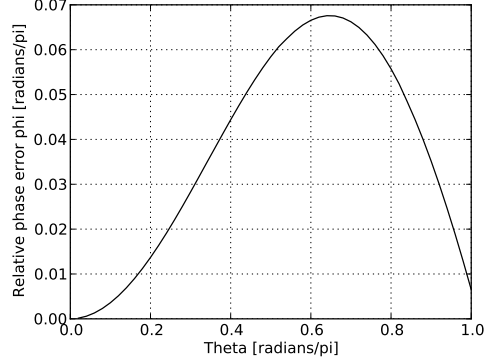


Figure 9:  $\Delta\phi$  Phase Error

### 3.2.2 Experimental Implementation

As we saw in figure 7, a Ramsey fringe is sensitive to the  $\epsilon$  phase error. Now that we have an operation that will amplify this error, we can insert one or multiple  $I_{\pi/2}$  operations in order to amplify the  $\epsilon$  phase error. This is the Amplified Phase Error (APE) sequence shown in figure 10.

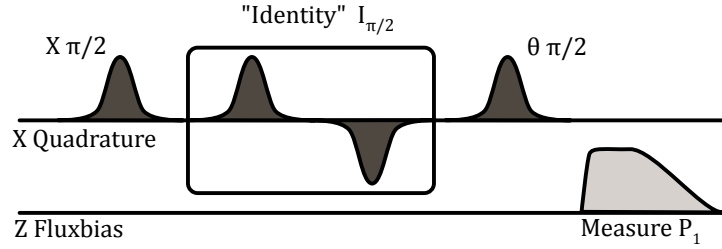


Figure 10: Amplifying Phase Error (APE) sequence

As is seen through matrix algebra in equation 8, each  $I_{\pi/2}$  identity acting on an equator state prepared by a  $X_{\pi/2}$ -pulse adds an extra  $\Delta\phi = 2\epsilon$  phase error. Repeating this  $I_{\pi/2}$  operation will add more phase error and increase the size of this effect.

$$|\psi\rangle = \frac{1}{\sqrt{2}} \begin{pmatrix} 1 \\ -i \end{pmatrix}, \quad I_{\pi/2}|\psi\rangle = \frac{1}{\sqrt{2}} \begin{pmatrix} 1 - 2i\epsilon \\ -i - 4\epsilon \end{pmatrix} \approx \frac{e^{-2i\epsilon}}{\sqrt{2}} \begin{pmatrix} 1 \\ -ie^{-2i\epsilon} \end{pmatrix} \quad (8)$$

Experimentally, we find that we can insert 5 identities before phenomena

such as  $T_1$ ,  $T_2$  and the nonlinearity of the  $\epsilon$  phase error give us adverse effects. This allows us to magnify the  $\epsilon$  phase error by roughly an order of magnitude, where we measure almost  $90^\circ$  of phase error as in figure 11. From the experiment, we find that is important to do a positive then negative  $\theta$  rotation for the identity operation to have the Bloch vector “bouncing” against the  $|1\rangle$  state rather than  $|0\rangle$ . It seems that doing so minimizes resetting of the qubit due to  $T_1$  relaxation and destroying phase error that we are trying to accumulate.

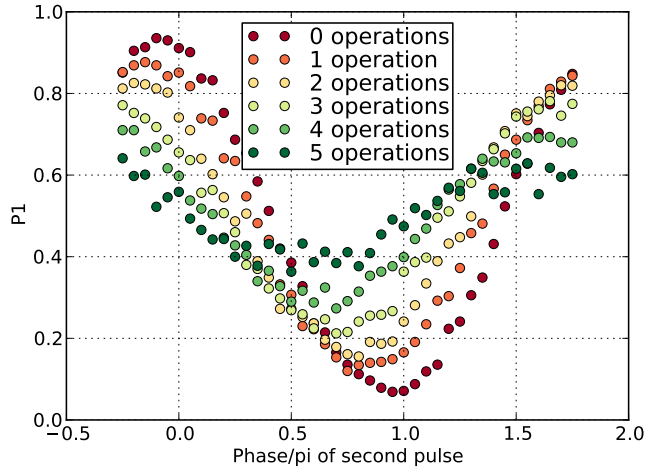


Figure 11: APE - Uncorrected phase error accumulation.

### 3.3 Phase Error Correction

#### 3.3.1 Derivative Removal by Adiabatic Gate (DRAG)

A technique known as Derivative Removal by Adiabatic Gate (DRAG)<sup>9</sup> has been developed by F. Motzoi et al. as a method of combating previously described gate errors. When performing a gate operation about the X quadrature, the Y and Z fluxbias remain idle. DRAG provides a way of using these idle degrees of freedom in order to dynamically detune the microwaves and qubit in a way that compensates for both the actual and virtual occupation

<sup>9</sup>Phys. Rev. Lett. 103, 110501 (2009)

of the  $|2\rangle$  state, preventing amplitude and phase errors. According to DRAG theory, one sets:

$$\mathcal{E}_y = -\frac{\dot{\mathcal{E}}_x}{\Delta} \quad \text{and} \quad \delta_1 = \frac{(\lambda^2 - 4)\mathcal{E}_x^2}{4\Delta} \quad (9)$$

where  $\mathcal{E}_y$  is the Y quadrature of microwaves,  $\delta_1$  is the qubit detuning,  $\Delta = 2\pi(f_{12} - f_{01})$  is the nonlinearity and  $\lambda = \sqrt{2}$  describes the relative strength between the 0-1 and 1-2 transitions. However, this triple control can be challenging as it requires using a separate Z fluxbias control in conjunction with both X and Y with precise timing and amplitude. In addition, generally these Z contributions are small and errors can arise from DAC discretization. However, it turns out that there is a convenient way of sidestepping this problem.

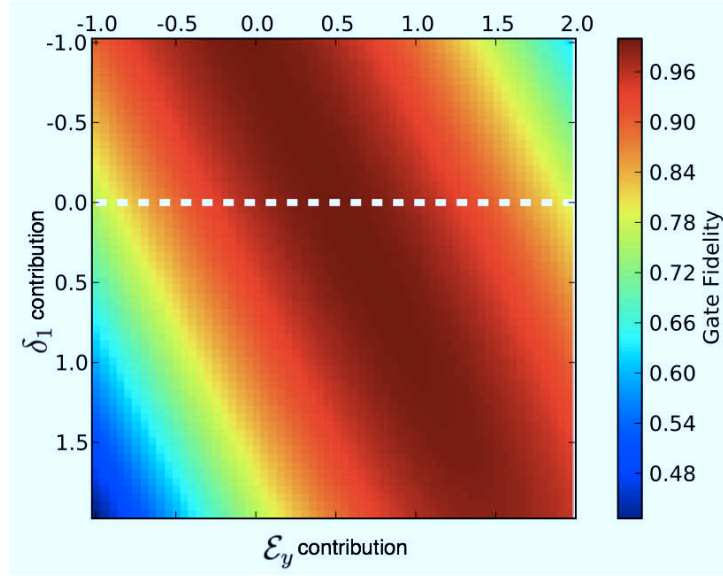


Figure 12: DRAG - Gate fidelity for combinations of Y and Z contributions. A value of 1.0 corresponds to the original theoretical value.

As is seen in the simulated data from figure 12, if we add coefficients to the  $\delta_1$  and  $\mathcal{E}_y$  contributions and modulate them, we find that they are both contributing similar effects to gate fidelity<sup>10</sup>. Rather than try to coordinate

<sup>10</sup>Gate fidelity is calculated as  $F = \text{tr}(\chi_{\text{simulation}}\chi_{\text{ideal}})$ , where  $\chi$  is calculated from quantum process tomography. See section 4.

two contributions at the same time, we can simply set  $\delta_1$  to 0 and calibrate the  $\mathcal{E}_y$  coefficient for an optimal value, which we find to be  $\frac{1}{2}$ . Doing so removes the Z-control and any associated calibration issues.

### 3.3.2 Half Derivative (HD) Method

Half Derivative (HD) method is based on the control theory of DRAG. It is named after the coefficient of  $\frac{1}{2}$  on the  $\mathcal{E}_y$  term, is given by:

$$\mathcal{E}_y = -\frac{\dot{\mathcal{E}}_x}{2\Delta} \quad \text{and} \quad \delta_1 = 0 \quad (10)$$

For a single qubit in ideal circumstances such that  $\mathcal{E}_x/\Delta$  is small, HD can be directly applied and does not require any tuning.<sup>11</sup> As is visible in figure 13, we can see that HD corrects for large amounts of the phase error, keeping the maxima and minima of  $P_1$  close to  $\theta = 0$  and  $\theta = 1$  respectively.

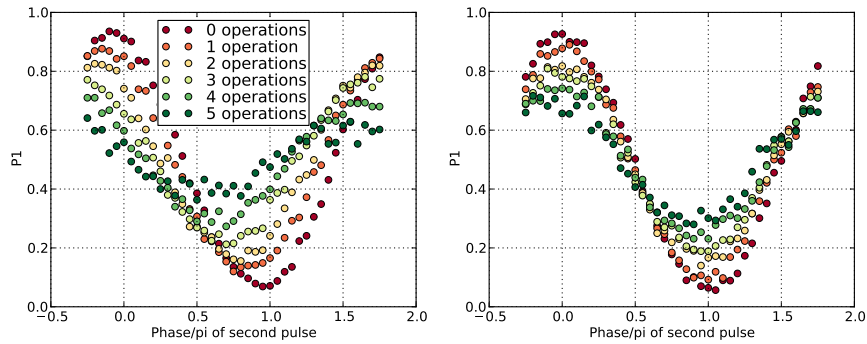


Figure 13: APE - Single-quadrature Gaussian (left) and HD (right).

To get a more intuitive picture as to just how HD improves the qubit gates, we can use state tomography to map out the gate trajectory along the Bloch sphere. We increase the amplitude of a pulse from 0 to  $\pi$ , and perform state tomography at each amplitude step. We then map the state back onto the Bloch sphere.

As can be seen in figure 14, a one quadrature Gaussian suffers amplitude and phase errors as the trajectory drifts away from the pole of the Bloch

<sup>11</sup>The amplitude may need to be re-calibrated for HD pulses as it can differ slightly, around 1%, from a single-quadrature Gaussian.

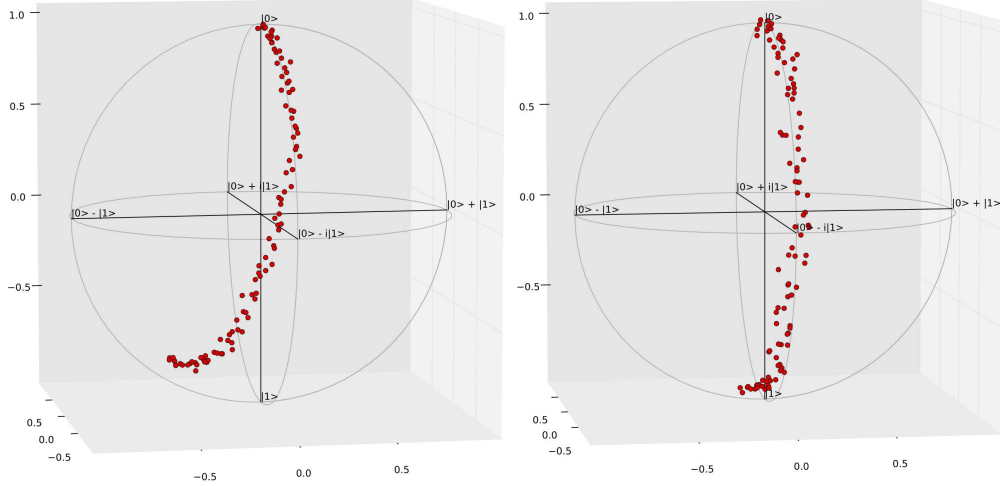


Figure 14: Bloch Sphere Trajectory - Gaussian (left) and HD (right)

sphere. This effect is dramatic using tomography, but  $P_1$  masks just how significant of an error this as at the pole of the Bloch sphere since  $P_1$  is first order insensitive to phase errors. In the HD pulse, the trajectory is directly down the meridian and appears to have greatly reduced phase error. HD is the ideal computational pulse that we seek.

To alleviate any last concern that we may have about this HD technique for improving microwave pulses, we may use quantum process tomography to compute a  $\chi$  matrix and overall gate fidelity, as in figure 18.

### 3.3.3 Caveats and Tunability

When deriving the math behind DRAG and HD, an assumption is made that  $\frac{\epsilon_x}{\Delta} \ll 1$  in order to perform a Taylor expansion. However, even in the most ideal cases when operating a phase qubit, this is not necessarily the case. When using shorter pulses such as a full width half maximum time of 5 ns, and with a relatively large  $\Delta = 2\pi(200 \text{ MHz})$ , we find  $\frac{\epsilon_x}{\Delta} \approx \frac{1}{2}$ , which is hardly a small parameter. The basic mathematics still hold fairly well even in these extreme circumstances, but with a smaller nonlinearity (such as  $\frac{\Delta}{2\pi} = 100 \text{ MHz}$ ) the expansion breaks down. In this case, HD can still dramatically improve qubit gates.

Rather than worry about the HD protocol in this limit, we can take the

basic idea and simply tune the correction for best performance. We insert a coefficient  $\alpha$  in front of the Y quadrature component and tune this parameter to an optimal value. Under normal circumstances,  $\alpha = \frac{1}{2}$ , but in less ideal limits, we can use the APE sequence to tune  $\alpha$  in a way that minimizes phase error.

In summary, we can use the following protocol for HD in the limit of short pulses or small nonlinearities:

$$\mathcal{E}_y = -\alpha \frac{\dot{\mathcal{E}}_x}{\Delta} \quad \text{and} \quad \delta_1 = 0 \quad (11)$$

Where  $\alpha$  is tuned to remove phase error on the APE sequence. We find a value typically within 20% of  $\frac{1}{2}$ . There are two types of dominant errors;  $|2\rangle$  state errors which are minimized by Gaussian pulses, and phase errors that which can be removed by tuning  $\alpha$ . Thus we can easily maximize gate fidelity with these methods.

## 4 Quantum Process Tomography

### 4.1 Formalism

Methods such as APE only probe specific aspects of our microwave control, such as phase errors. In order to get a complete picture of our gates we can use Quantum Process Tomography (QPT). This mathematical framework can be used to completely describe the transformation independent of the input state.

The methodology for describing a qubit gate is as follows. We wish to describe the transformation in a complete and general way by inserting some initial state  $\rho$  and the transformation returns some different state  $\mathcal{E}(\rho)$ .

$$\mathcal{E}(\rho) = \sum_{mn} E_m \rho E_n^\dagger \chi_{mn} \quad (12)$$

Where  $\{E\}$  form a basis for the set of operations on  $\rho$ . The  $\chi_{mn}$  scalars weigh each individual process labeled by  $m, n$ . The  $\chi$ -matrix itself therefore completely describes the process in some basis of  $\{E\}$ . This kind of formalism is essential as decoherence errors prevent the transformation from being truly

unitary. Consult *Quantum Computation and Quantum Information*<sup>12</sup> for more detail.

## 4.2 Experimentally Constructing $\chi$

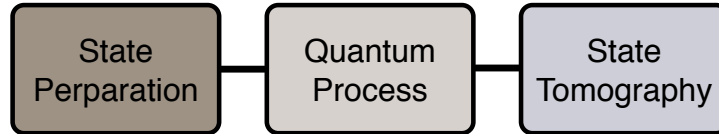


Figure 15: Quantum Process Tomography

The next step is experimentally determining what the  $\chi$ -matrix for a qubit gate and compare it to the ideal, an overview of the experimental procedure is given in figure 15. This can be done by initializing the qubit in various input states that span the space of possible states, transforming the state with a qubit gate, and performing tomography such as in figure 16 to reconstruct the state afterwards. By using tomography on the initial set of basis states and the states after the transformation, we can reconstruct what the transformation does independent of input state by computing the  $\chi$ -matrix by the process shown in figure 17. For further detail on experimental process tomography, see M. Neeley et al. *Nature Physics* 4, 523-526 (2008).

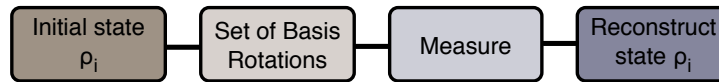


Figure 16: State Tomography - The set of basis rotations rotate the state such that each measurement will be equivalent to projecting the state on orthogonal axes.

Once we have obtained a  $\chi$ -matrix, we may compute the operation fidelity defined as  $F = \text{tr}(\chi_{\text{experiment}}\chi_{\text{ideal}})$ . We may also view the matrix to get specific error information; the  $\chi$ -matrix tells us all the desired and undesired operations that occur in the transformation. Figure 18 shows experimental data for both HD and single-quadrature Gaussian  $\pi$ -pulses.

<sup>12</sup>Nielsen, M.A. & Chuang, I.L.. *Quantum Computation and Quantum Information* (Cambridge Univ. Press, Cambridge, 2000).

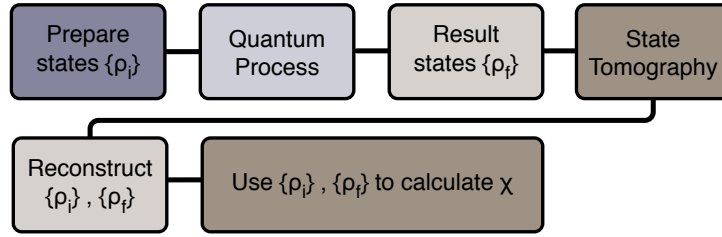


Figure 17: Calculating  $\chi$

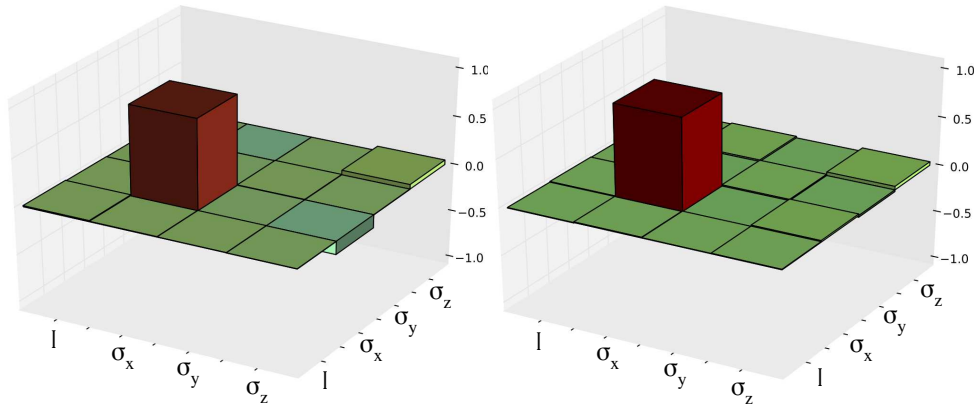


Figure 18: Quantum Process Tomography - Real part of the  $\chi$ -matrix for single-quadrature Gaussian (left) and HD (right) in the Pauli  $\{I, \sigma_x, \sigma_y, \sigma_z\}$  basis. The only ideal matrix component is the  $\sigma_x, \sigma_x$  component. Notice how HD corrects for the  $\sigma_z, \sigma_x$  error process. Imaginary components of the  $\chi$ -matrix not shown as error elements are small and not strongly effected by HD.

## 5 Flux Bias Calibration: Z control

Up through this point, we have high fidelity control for any X or Y gate, as well as any combination of the two. However, what has gone completely untouched is Z control. Fortunately, once the microwaves are tuned up this becomes relatively straightforward. The Z control works by changing the relative phase between the  $|0\rangle$  and  $|1\rangle$  state, but does not excite any transitions between them. The challenge in tuning up Z gates is that to read out the qubit we measure  $P_1$ . Since Z gates do no directly effect this value, we must

use a slightly more complex calibration procedure from X and Y gates.

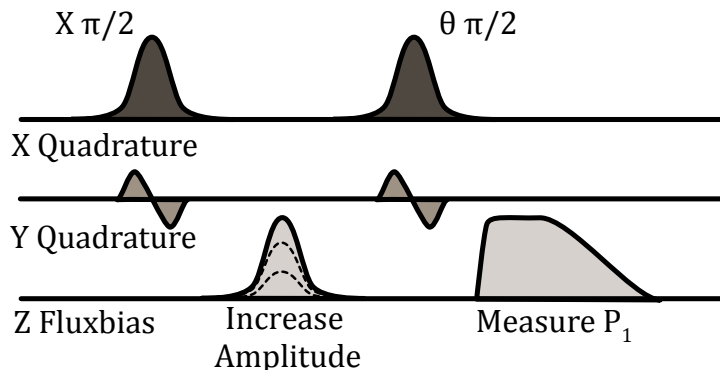


Figure 19: Z calibration sequence

These conditions present a natural sequence which calibrates the Z amplitude along the Bloch equator, shown in figure 19. The idea is to rotate the Bloch vector to the equator with a  $X_{\pi/2}$ -pulse, increase the amplitude of a fixed length Z pulse and perform another  $X_{\pi/2}$ . If the correct amplitude for a  $Z_{\pi}$  pulse is used, the second  $X_{\pi/2}$  will be completely out of phase with the first. This returns the qubit to the ground state, as in figure 20. At this point we will note why it was so important to calibrate the qubit frequency so precisely and to remove phase errors from the X and Y gates. Without the precise bring-up that we followed, we would have phase errors from the X gates in our Z tune up procedure. This would give us errors in calibrating Z gate amplitude, as phase errors combine additively with Z gates.

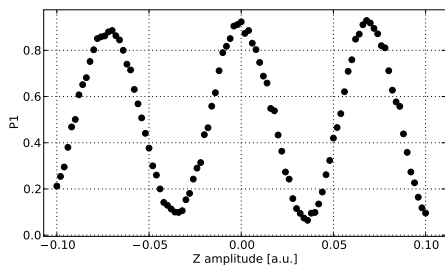


Figure 20: Z calibration data - Notice the minimum in  $P_1$  around the amplitude of 0.035.

As the Z control does not excite any transitions between states, we do

not have to worry about virtual or actual occupation of a 3rd state such as during the X and Y gates. This is why no technique such as HD is required for Z gates, and a simple Gaussian pulse will do.

## 6 Randomized Benchmarking

### 6.1 Pulse Sequence

Now that the qubit is tuned up, we can use the technique of Randomized Benchmarking developed by Knill et al.<sup>13</sup> and carried on superconducting qubits by J. M. Chow<sup>14</sup> as a way of getting an averaged measure of qubit gate error. The technique essentially is a method of averaging over all different types of qubit gates to get a single number representing the qubit fidelity. As this is a benchmarking that is averaging essentially all errors, it is not particularly useful as a tune up procedure, but it is a nice final check after all tune up has been performed to quantify how a device is performing. This has advantages over tomography as it averages over all computational gates and does not scale exponentially with the number of qubits, as tomography does.

The protocol involves a pulse sequence  $R_f \prod_i C_i P_i$ , where  $P_i$  are Pauli rotations ( $\pi$ -pulses) and  $C_i$  are Clifford group generators ( $\frac{\pi}{2}$ -pulses), and  $R_f$  is a final  $\frac{\pi}{2}$ -pulse. The idea is to randomly generate a series of uncorrelated, interleaved  $\pi$  and  $\frac{\pi}{2}$ -pulses of any axis or direction to test all the potential operations of the qubit. However, we want to be able to determine the fidelity of all of these operations, and we do not want to have to perform state tomography<sup>15</sup> at the end of a sequence. The purpose of the  $R_f$  pulse is to rotate the Bloch vector onto the Z axis<sup>16</sup> so that a simple  $P_1$  measurement can be used to determine fidelity. Then, we can perform multiple tests of various lengths to get an idea of how overall fidelity drops over numerous gate operations, and use this information in order to determine the average error associated with each gate.

Rather than randomizing every single operation, we take the approach

---

<sup>13</sup>Phys. Rev. A 77, 012307 (2008)

<sup>14</sup>Phys. Rev. Lett. 102, 090502 (2009)

<sup>15</sup>See section 4.2.

<sup>16</sup>If the Bloch vector is already aligned with the measurement axis, an identity operation is performed.

of generating a long random sequence, and probing the fidelity after every iteration within it. First, we generate the longest sequence that we wish to check by generating a list of variables that determine the axis and rotation of each pulse in that sequence. This list will determine all of the pulses minus the  $R_f$  pulse. The challenge is determining the fidelity at various points within the sequence, when the Bloch vector is not necessarily aligned with the  $Z$  axis. We then truncate the sequence up to some number of  $\pi$ ,  $\frac{\pi}{2}$  iterations and tack on the corresponding theoretically calculated  $R_f$  pulse that will bring the Bloch vector to the  $Z$  axis. This gives us the fidelity of the sequence after some number of iterations. This process is described in figure 21.

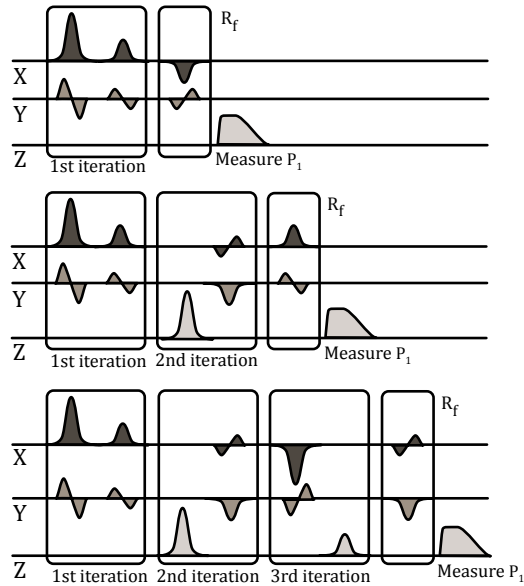


Figure 21: Randomized Benchmarking - Probing the fidelity as various points in a long sequence. Measuring the fidelity after 1, 2, and 3 iterations of  $\pi$ ,  $\frac{\pi}{2}$ -pulses. Notice how  $R_f$  changes after each sequence, as it is calculated by each particular sequence to move the Bloch vector to the  $Z$  axis.

## 6.2 Experimental Implementation & Analysis

After testing many different sequences and checking the fidelity after each iteration, we plot the fidelity and expect to see an exponential decay due to

decoherence and gate error accumulation. We know that at zero iterations, the fidelity should be at 1.<sup>17</sup> We also expect that after many iterations, the fidelity should reside around 0.5. Given these assumptions, we may simply fit the parameter  $b$  in the exponential  $F = 0.5e^{-bn_i} + 0.5$ . This functional form gives us the exponential behavior we seek as well as the boundary conditions that we stipulate. The variable  $b$  then can be interpreted as the “error per iteration”. As each iteration has 2 gates,  $b/2$  gives us an average “error per gate” that we wish to quantify. Figure 22 shows experimental data for randomized benchmarking, as well as the exponential fit.

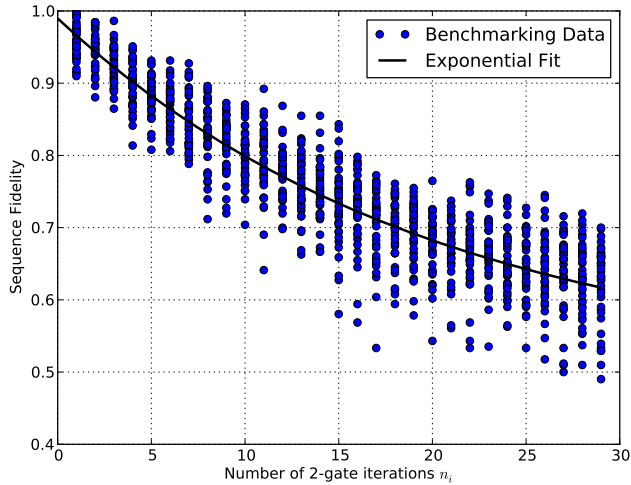


Figure 22: Randomized Benchmarking - Experimental data for 40 different sequences. Variance in fidelity is consistent with statistics for 600 experiments per data point. Gates are 5 ns full width half maximum with 7 ns between the center of each gate.

Notice that the exponential fit in figure 22 does not go exactly to 1 as iterations goes to 0. This data set was least-squares fit to a two parameter function:  $F = Ce^{-bn_{iterations}} + 0.5$ . This is a way to double check that our measurement correction is behaving as we expect. For this experiment, we find that  $C = 0.490$  and  $b = 0.0494$ . This value of  $C$  within 2% to the ideal

<sup>17</sup>This assumes no measurement error. In this case, we have corrected for measurement error to validate this assumption. For more on measurement error correction, see the supplemental information of R.C. Bialczak et al. arXiv:0910.1118v1

value of 0.5 is consistent with accurate measurement error correction. The value of  $b$  corresponds to an experimental “error per gate” of 2.47%, where we consider each iteration in the protocol as 2 gates.

## 7 Gate Timing

Now that we have carefully tuned microwave gates and have a standard for computing gate and sequence fidelity in an precise way, we can begin to consider more complicated multi-gate experiments. Previously, we were trying to extract useful information out of experiments. During tune up procedures, it is important to keep qubit gates well separated as we want to avoid overlap errors at the cost of suffering more greatly from predictable errors such as  $T_1$  and  $T_2$ . As we move forward, we can begin to consider how optimize for every last bit of fidelity out of our qubits.

Currently, the greatest source of error in any quantum algorithm comes from decoherence. With this in mind, each experiment is some what of a “race against time”, where we try to accomplish as much as we can before decoherence destroys all information in the qubit. To combat this, we can push our gate operations closer together and make individual gates shorter. However, it is important to strike a balance between overlapping gates and decoherence, as either can generate substantial errors. Given that a Gaussian has infinite extent unless we truncate it, the question becomes just how close together do we place them?

By varying the gate delay in randomized benchmarking, we notice that there is a point where gates are spaced too closely together as the fidelity of certain sequences plummets, quickly dragging down the average error per gate, as seen in figure 23. Randomized benchmarking is not a tune up procedure per se, but it can be useful in finding correct gate spacing in general as it provides a “global” approach to testing virtually every kind of sequences for a set of parameters.

Process tomography provides us a metric for optimizing individual sequences, and again can provide a method for optimizing gate delay, in a similar vein to randomized benchmarking.

Although these methods are not particularly elegant, they provide a precise way of combating a complicated problem.

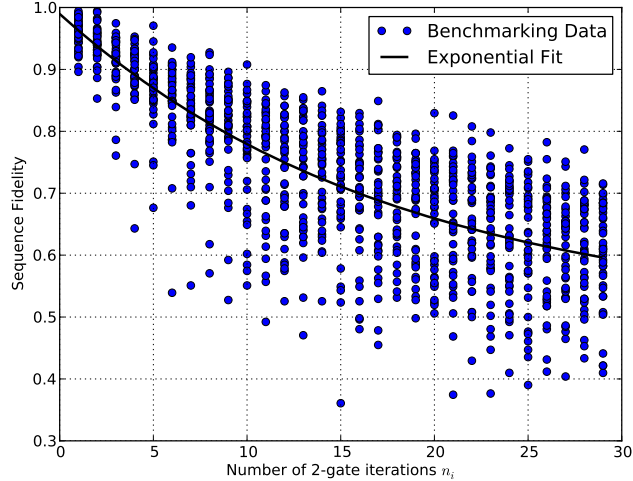


Figure 23: Randomized Benchmarking - Overlap errors greatly reduce fidelity of some sequences, as seen by the overall drop in fidelity and increase in variance. In this data, gate delay is 6 ns as opposed to 7 ns previously. All other parameters are identical to figure 22. An overall drop in “error per gate” is seen as  $b = 0.0562$ .

## 8 Conclusions & Moving Forward

In the process of bringing up and calibrating a qubit, we find bootstrapping to be an essential aspect in the procedure. We are able to discover and optimize fundamental aspects of a qubit via clever experimentation and careful analysis. In addition, we have built on previous work by developing the APE sequence to better measure phase errors, and implemented DRAG in an experimentally convenient way in order to correct for them.

At this point we have a tuned up single qubit for all relevant computational gates. Through process tomography and randomized benchmarking we also have a good idea how each gate is working. Although everything should be working precisely at this point, we have several tools for inevitable troubleshooting that will be required in performing an experiment.